Nanoscale

Open-Air Spray Plasma Deposited UV-Absorbing Nanocomposite Coatings

Journal:	*Nanoscale*
Manuscript ID	NR-ART-05-2018-004095.R1
Article Type:	Paper
Date Submitted by the Author:	11-Jul-2018
Complete List of Authors:	Ding, Yichuan; Stanford University, Materials Science and Engineering Dong , Siming; Stanford University, Materials Science and Engineering Hilt, Florian; Stanford University, Materials Science and Engineering Dauskardt, Reinhold H.; Stanford University, Materials Science and Engineering

Article type: Full Paper

Open-Air Spray Plasma Deposited UV-Absorbing Nanocomposite Coatings

*Yichuan Ding, Siming Dong, Florian Hilt, and Reinhold H. Dauskardt**

Department of Materials Science and Engineering, Stanford University, Stanford, CA, 94305-2205, USA
E-mail: dauskardt@stanford.edu

Keywords: transparent protective coatings, open air plasma deposition, ultrasonic spraying, nanocomposite, UV-protection, hardness

Abstract

We demonstrate the deposition of mechanically robust UV-absorbing nanocomposite coatings with a newly developed dual-source deposition method involving ultrasonic spraying and open-air plasma deposition. Nanoparticles and the coating matrix are independently deposited which eliminates difficulties associated with preparing composites with high mass fraction of well-dispersed nanoparticles in the matrix. Nanocomposite coatings containing different concentrations of silica, ceria, and both titania and ceria nanoparticles were successfully deposited with good nanoparticle dispersity, high transparency over the visible range, effective absorption in the UV wavelength, and enhanced mechanical properties. Moreover, films were successfully deposited on several substrates including polycarbonate to demonstrate the low processing temperature of this dual-source deposition method. Coatings with different nanoparticle concentrations and film thicknesses were systematically studied in terms of their surface morphology, optical properties and mechanical properties. Accelerated photostability testing of the UV-absorbing nanocomposites demonstrate significantly enhanced performance compared to existing coatings with either a polymeric matrix or organic UV-absorbers.

1. Introduction

Open-air plasma deposition (OAPD) is an emerging technique that enables open-air plasma deposition of coatings on large and/or complex geometry substrates without the need for expensive vacuum or inert manufacturing platforms. [1-3] The active species including free radicals, metastables, UV light, and convective heating, created by the plasma assist the film formation at low deposition temperatures (< 60°C) that is applicable for plastic and organic substrates. Recent studies have demonstrated its capability for depositing highly transparent organosilicate coatings on plastics with tunable mechanical properties that are superior to the commercial sol-gel coatings.[4-6] Moreover, with OAPD, the substrate surface is functionalized simultaneously during film deposition which can lead to better interfacial properties.[7-9] The significantly improved film adhesion and hardness translates into improved durability and resistance to scratching and environmental degradation.

In this work, the OAPD system is combined with ultrasonic spraying for depositing high performance, multifunctional nanocomposite (NC) coatings. While the plasma deposited matrix provides enhanced adhesion to the substrate along with durability and resistance to scratching and environmental degradation, the embedded ultrasonic sprayed nanoparticles by can impart a variety of functionalities to the coating. Recent studies have demonstrated the application of nanoparticles as mechanical reinforcements,[10, 11] catalysts,[12, 13] UV-absorbers,[14, 15] biological imaging agents,[16] and others. The properties of the nanoparticles depend on factors such as their shape,[17] surface chemistry,[13, 18] size,[13, 19, 20] and strain state.[21] When incorporated into a matrix, their dispersity and interfacial interaction with the matrix may also play important roles in the overall functionality, performance and reliability of the resulting NC.[10, 22, 23]

For making NC coatings, nanoparticles are generally incorporated by either in-situ growth in the matrix [24] or by dispersing into the matrix precursor before deposition.[10, 25] In our dual-source deposition method, the nanoparticles and matrix are independently deposited to eliminate the potential difficulties associated with preparing high mass fraction composites with well-dispersed nanoparticles. It also allows for depositing NC coatings containing one or more types of nanoparticles with both in-plane and through thickness uniformity. Moreover, the simultaneous surface activation during film deposition by plasma can enhance the interfacial properties at the matrix-nanoparticle interface which is crucial for enhanced mechanical properties.[22, 23, 26]

Silica (SiO_2), ceria (CeO_2), and titania (TiO_2) nanomaterials are all important functional materials that have been recently studied as mechanical reinforcements,[10] UV absorbers,[14, 15] photocatalysts,[27, 28] photodetectors,[29] and adsorbent for toxic heavy metal ions.[30] Here we demonstrate NC coatings containing silica (SiO_2), ceria (CeO_2), and both titania (TiO_2) and CeO_2 nanoparticles with high transparency in visible wavelengths, strong absorption of UV light, and enhanced mechanical properties. Films with different nanoparticle concentrations and thicknesses were systematically studied and characterized with high resolution techniques. Accelerated UV exposure tests were also performed on the UV-absorbing coatings, and the results demonstrated outstanding film photostability that are significantly better than existing coatings with either a polymeric matrix or with organic UV-absorbers. Films with selected nanoparticle concentrations were successfully deposited on a polycarbonate (PC) substrate to demonstrate the low processing temperature capability. Due to its enhanced mechanical and UV-absorbing properties compared to the commercial sol-gel coatings and organosilicates deposited

by OAPD alone, the NC coating has the potential to better protect polymer substrates against mechanical and photo-degradation.

2. Results and discussions

2.1. Deposition of the SiO_2 NC coatings

2.1.1. Depositing SiO_2 nanoparticles without the coating matrix

The nanoparticle dispersity on the substrate was studied using a well-dispersed SiO_2 nanoparticle suspension solution (0.025 mg/ml) sprayed onto a silicon substrate without plasma. The size distribution profiles of the SiO_2 nanoparticle dispersion in water was measured by dynamic light scattering (DLS) and an average size of 23 nm with a poly-dispersity index (PDI) of 0.181 were determined (**Figure S1a** in Supporting Information). Scanning electron microscope (SEM) micrographs (**Figure S2a**) revealed nanoparticles on substrate of ~25 nm in diameter, which is consistent with the DLS measurements and proved the uniform dispersion of nanoparticles over the substrate without any substantial agglomerations. SEM images with lower nanoparticle coverage were used for determining the nanoparticle deposition rate.

2.1.2. Surface Morphology of the SiO_2 NC coatings

NC coatings containing ~10 wt.%, ~20 wt.% and ~30 wt.% of SiO_2 nanoparticles were deposited onto silicon substrates using the combined ultrasonic spray and OAPD method. A schematic of the instrument setup is illustrated in **Figure 1** with all detailed processing conditions summarized in **Table 1**. Processing procedures were described in detail the Experimental section. For depositing high quality films with minimum haziness and maximum transparency, a good dispersity of the nanoparticle was necessary. Moreover, during each pass, after nanoparticle deposition, a complete solvent evaporation before matrix deposition was

necessary to prevent any pinhole formations. In this work, the travel time between the two deposition sources was 2 seconds, considerably larger than the droplet evaporation time, tens of milliseconds, as previously reported.[31]

Figure 2a shows a representative cross-sectional SEM image of the NC films containing 20 wt.% nanoparticles. The film thicknesses was determined to be ~320 nm and a granular surface morphology was revealed. These protruding granular microstructures resulted from the nanoparticles near the surface that were not fully flattened or embedded into the coating matrix, and these microstructures became more obvious when the nanoparticle inclusion concentration increased. **Figure 2b** shows a representative top-view SEM image of the 20 wt.% NC coating. A uniform distribution of the SiO_2 nanoparticle in the coating matrix was revealed with insignificant agglomeration even at a high weight fraction. This is important for the properties of NC coatings as nanoparticles agglomeration usually results in adverse effects on the thermal and mechanical properties of the coating matrix.[22, 32]

Atomic force microscope (AFM) was employed to quantify the roughness of the NC films and **Figure 2c** shows a typical AFM micrograph of NC coatings containing 20 wt.% nanoparticles. The film became rougher with increasing nanoparticles inclusions and the root-mean-squared (r.m.s) surface roughness increased from 4 nm to 9 nm and to 19 nm when nanoparticle concentrations increased from 10 wt.% to 20 wt.% and to 30 wt.%. Slight coffee-ring effect were observed and became more significant for films containing more nanoparticles. These rings were also observed during nanoparticle spraying without plasma, and were more obvious when higher concentration dispersions were used. However, the rings were only tens of nanometers in height so did not significantly affect the film quality. For comparison purposes,

the AFM micrographs of the coating matrix containing no nanoparticle were measured and the r.m.s roughness was determined to be 1 nm.

2.1.3. Optical properties of the SiO_2 NC coatings

Transmittance of the SiO_2 NC coatings on glass with different nanoparticle inclusion concentrations was measured (**Figure 3**). A blank glass substrate was used as the reference. The coating matrix employed is highly transparent and showed a ~100% transmission over the visible region. All NC coatings exhibit > 92% transmittance in the visible range even at a high weight fraction of 30 wt.%. Coatings with 10 wt.% nanoparticle inclusion showed even higher transmittance than the coating matrix. This can be attributed to the fact that both the NC film and the coating matrix are optically thin so that thin film interference played a role. At wavelength of 550 nm, the transmittance only decreased by 1% and 3% for 20 wt.% and 30 wt.% NC coatings compared to the coating matrix, respectively. The transmittance decreased at lower wavelength as light scattering became more significant especially for the 30 wt.% film where nanoparticles started to percolate. The overall high transmittance further proved a good dispersity of nanoparticles within the coatings especially for the 10 wt.% and 20 wt.% films.

2.1.4. Mechanical properties of the SiO_2 NC coatings

Figure 4a shows the elastic modulus of the NC coatings with different nanoparticle concentrations. Every data point on the plot corresponds to the value measured from a specific location on the specimen and at least 16 individual points were tested for every specimen. Scatter of the measured values originated from the local modulus variation of the NC film. Since the indenter tip is sharp (~100 nm in diameter), the measured value was considerably higher when nanoparticles were present in the vicinity of the contact area. The plasma deposited coating matrix showed an average elastic modulus of 14.0 GPa, which is about 2.5 times higher than the

commercial sol-gel polysiloxane coatings.[6] This enhancement can be attributed to the increasing molecular network connectivity within the film arising from the plasma-enhanced oxidation reaction in the afterglow region.[5, 6]

The average elastic modulus increased from 14.0 GPa to 21.7 GPa at 10 wt.% and to 24.9 GPa at 20 wt.%. The enhancement was mainly caused by the incorporation of the stiffer secondary phase, *i.e.* SiO_2 nanoparticles. In addition to that, the strong interactions between the coating matrix and the nanoparticles can also be important as it assists the load transfer from the matrix to the nanoparticles.[22, 23, 32] The strong interfacial interactions are achieved due to 1) the activation of the nanoparticle surface during plasma exposure,[8, 33, 34] 2) enhancement of the silane precursor wetting during deposition, and 3) increased reactivity of the silane precursor when activated by the active plasma species (eg. free radicals, metastables, UV-light, etc.). Moreover, direct evidence of covalent bond formation at the silane-metal interface during OAPD was previously reported using time-of-flight secondary ion mass spectrometry.[35]

The average elastic modulus decreased to 18.3 GPa at 30 wt.%. Also note that some values measured for the 30 wt.% film were below the lowest value measured for the coating matrix, suggesting the coating matrix became weaker when 30 wt.% of nanoparticles were incorporated. This deterioration can be attributed to the potentially increased porosity or micro-voids formed in the film when the nanoparticles loading is high.[36] The increased roughness caused by the coffee ring effect can also result in this decrement in the elastic modulus.

The hardness of the films showed a similar trend as indicated by **Figure 4b**. The average hardness increased from 0.9 GPa for the coating matrix to 1.4 GPa at 10 wt.% and to 1.7 GPa at 20 wt.% and then decreased to 1.2 GPa at 30 wt.%. This enhancement of the film elastic modulus and hardness can potentially result in better abrasive wear resistance and scratch

resistance as reported in literature and can be very important for applications such as protective coatings on plastics.[37-39]

2.2. Deposition of the CeO_2 NC coatings

The versatility of this co-deposition process allows us to deposit NC coatings containing other types of nanoparticles with similar processing parameters. Here, deposition of CeO_2 NC coatings were demonstrated as an example using the same method and processing conditions as for SiO_2 NC coatings except that a CeO_2 dispersion was used for spraying. **Figure S1b** shows the size distribution profile of the CeO_2 nanoparticle dispersion and an average size of 112 nm with a PDI of 0.127 was determined.

2.2.1. Surface Morphology of the CeO_2 NC coatings

Figure 2d and **2e** display typical cross-sectional and top-view SEM images of a 20 wt.% CeO_2 NC coating on silicon substrate, respectively. The cross-sectional micrographs exhibit a coating thickness of ~320 nm with similar granular surface morphologies as observed on SiO_2 NC films. As mentioned earlier, these protruding granular microstructures are resulted from those not fully embedded or flattened nanoparticles near the coating surface. The top-view image showed that these granular microstructures ranged from 50 to 200 nm in size, which is similar to the size of the CeO_2 nanoparticles determined by the DLS (**Figure S1b**). It suggests that no obvious aggregation of nanoparticles occurred during OAPD. The granular microstructures observed here are larger in size compared to the ones on the SiO_2 NC coatings mainly because the CeO_2 nanoparticles are larger in size as determined by the DLS. AFM micrographs were collected for determining the surface roughness and the corresponding images were shown in **Figure 2f**. The r.m.s roughness was determined to be 28 nm which is greater than the SiO_2 NC

coatings with similar thickness and weight fraction. Since the film roughness originated from the protruding granular microstructures, the larger CeO_2 nanoparticle is believed to cause the rougher surface.

2.2.2. Optical properties of the CeO_2 NC coatings

CeO_2 NC coatings with different film thicknesses were deposited on quartz substrates by varying the deposition cycles. The transmission spectra of these films were measured using a blank quartz substrate as the reference. As shown in **Figure 5**, the coating matrix is >94% transparent in the UV wavelength (*i.e.* 200-400 nm). In comparison, the NC coatings exhibit stronger absorption of UV-radiations with increasing film thickness, and strong absorptions in the UV-B (*i.e.* 280-315 nm) and UV-C (*i.e.* 200-280 nm) ranges with a local maxima at wavelength of 305 nm was observed. In the visible range, all coatings show good transparency without any detectable yellowish coloration originated from CeO_2. At wavelength of 550 nm, the transmittance only decreased for 3%, 6%, and 8% for ~220 nm, ~415 nm, and ~510 nm thick coatings, respectively.

2.2.3. Photostability of the CeO_2 NC coatings

In order to determine the photostability of the CeO_2 NC coatings, an accelerated UV test was performed by exposing a ~510 nm thick film on quartz to intensified UV-B radiation (~60 W/m^2) while monitoring the absorption at 305 nm (wavelength corresponding to the local maximum absorption) *vs.* the exposure time. As shown in **Figure 6a**, the normalized absorbance at 305 nm stays higher than 0.91 after 100 hours of intensified UV exposure, suggesting the durability of the NC coating is significantly better than coatings made with organic UV-absorbers embedded in sol-gel derived matrices for which the normalized absorbance dropped below 0.9 only after 5 hours of UV exposure with a smaller UV-B dosage (40 W/m^2).[40]

The improved photostability was attributed to the reduced photo-degradation and photo-desorption of the inorganic nanoparticle compared to the organic UV-absorbing molecules. The transmittance in the visible range also exhibits no deterioration with the intensified UV-exposure. As shown in **Figure 6b**, the transmittance at wavelength of 550 nm stay almost the same if not slightly higher after 100 hours exposure. No yellowing or cracking was observed after the UV-radiation visually or by the high magnification optical microscope (**Figure S3**). This demonstrates an improved photostability of the plasma deposited coating matrix as compared to most of the polymer matrices which could be quickly degraded by UV-irradiation especially when photocatalyzed by the inorganic nanoparticles.[41, 42]

2.2.4. Mechanical properties of the CeO_2 NC coatings

The incorporation of CeO_2 nanoparticles also leads to an improvement of the film stiffness. The 20 wt.% film exhibits an average elastic modulus of 18.2 GPa and an average hardness of 1.2 GPa (**Figure S4**), which are ~30% higher than the coating matrix and are more than 3 times higher than the commercial sol-gel polysiloxane coatings.[6] Therefore, in addition to be UV-protective, the film is also mechanically stiff, making it a promising candidate for polymeric substrate protections.

2.3. Deposition of the CeO_2 - TiO_2 NC coatings

The dual spray-OAPD method is also capable of depositing coatings with more than one type of nanoparticles. Here, coatings containing both TiO_2 and CeO_2 nanoparticles are deposited using a mixed dispersion containing both TiO_2 and CeO_2 nanoparticles for spraying. **Figure S1d** shows the size distribution of the mixed dispersion (1 : 1 by weight) after diluted with deionized water to a total concentration of 1 wt.%. It shows an average size of 98 nm with a PDI of 0.196.

Compared to the CeO_2 dispersion and TiO_2 dispersion (**Figure S1c**, average size of 84 nm with a PDI of 0.175), the mixed dispersion has an average size in between with a greater PDI value, which suggests that the two types of nanoparticles are compatible and no further aggregation was happened during the mixing. It was further confirmed by spraying the mixed dispersion (0.025 mg/ml) onto silicon substrate without plasma, and the SEM images (**Figure S2c**) indicate a similar average size as compared to the DLS measurements.

2.3.1. Surface Morphology of the CeO_2 - TiO_2 NC coatings

Figure 2g and **2h** show typical cross-sectional and top-view SEM images of the NC coatings containing 10 wt.% CeO_2 + 10 wt.% TiO_2 deposited on silicon substrate, respectively. The film thickness is ~ 320 nm with similar granular surface morphology as observed on other NC coatings. AFM micrograph (**Figure 2i**) measured the r.m.s roughness to be 34 nm, which is larger than that of SiO_2 NC coatings and is similar to the CeO_2 NC coatings with similar thickness and weight fraction. It further suggests that the roughness originated from the protruding granular microstructures and the larger the nanoparticles size, the rougher the film.

2.3.2. Optical properties of the CeO_2 - TiO_2 NC coatings

The specular transmission spectrum of a NC film containing 10 wt.% CeO_2 + 10 wt.% TiO_2 was measured by using a blank quartz substrate as the reference. As shown in **Figure 5**, the film exhibits an increasing absorption of UV-A and UV-B wavelength while maintains similar transparency in the visible range as compared to the 20 wt.% CeO_2 NC coating which has a thickness of ~510 nm. Same accelerated UV test was performed and the film shows a slightly reduced photostability after 20 hours of exposure as compared to the CeO_2 NC coatings (**Figure 6a**). No yellowing or cracking was observed visually or by high magnification optical microscope after the UV-radiation.

2.3.3. Nanoparticle dispersity inside the coating matrix

Figure 7a – 7d illustrate scanning Auger microscope (SAM) elemental mapping of Ce, Ti, Si, and O in the NC coating containing 10 wt.% TiO_2 and 10 wt.% CeO_2 nanoparticles. The SEM image corresponding to the scanned area is shown in **Figure 7f**. Ti and Ce signals are only significant at localized regions where the nanoparticles are present. Si and O signals are uniformly distributed throughout the whole scanned area with local variations at regions where the nanoparticles are present. **Figure 7e** illustrates an RBG overlay image of the Si, Ti, and Ce. Note that, Ti and Ce regions are uniformly distributed on the whole scanned area, suggesting each kind of nanoparticles are uniformly dispersed in the coating matrix. Moreover, no significant correlations were found between Ce and Ti signals, suggesting the two kinds of nanoparticles are independently distributed. The effective particles size in the coating revealed by the SAM mapping is similar to the size determined by the DLS when particles were in the dispersions. It suggests that no aggregation of nanoparticles was occurred during nanoparticle deposition and during OAPD of the coating matrix. Compared to the NC coatings made by OAPD using a dispersion of nanoparticles in the matrix precursors where aggregates of several micrometers were present,[43] the nanoparticle dispersity made with this dual source method is significantly enhanced. This is important to achieve the optimized film properties as nanoparticle agglomerations can have negative impacts on the thermal, optical and mechanical properties.[22, 32]

2.4. Deposition of the NC coatings on PC substrate

The low processing temperature (< 90 °C) of this method allows us to deposit NC coatings on substrates which cannot tolerate high temperatures, such as polymer substrates or

organic thin films. Two optimal compositions (coating containing either 20 wt.% SiO_2 or 20 wt.% CeO_2) were selected for low temperature deposition on PC substrate with thicknesses ~320 nm.

Visually, these films exhibit great optical qualities without any haziness or coloration. The inset photograph shown in **Figure S5a** demonstrates that the films are highly transparent that the Stanford logo below the films can be clearly seen. **Figure S5b** and **S5c** show the AFM micrographs for the SiO_2 and CeO_2 NC coatings, respectively. The determined r.m.s roughness values are 7 nm for SiO_2 NC coatings and 26 nm for CeO_2 NC coating, which are similar to the films deposited on the silicon substrates. The specular transmission spectra of these films were measured by using a blank PC substrate as the reference and were shown in **Figure S5a**. Only the visible range is shown because the PC substrate is not UV-transparent. Both films had similar transmittance in the visible range as compared to those deposited on quartz or glass with a similar nanoparticle dispersity within the coating. The similar surface roughness, nanoparticle dispersity, and optical properties of the NC coatings deposited on PC substrates as compared to those on the inorganic substrates indicates that the dual-source deposition method was not substrate sensitive.

X-ray photoelectron spectroscopy (XPS) depth profiling was utilized to determine the through thickness chemical composition of the 20 wt.% CeO_2 NC coatings and was shown in **Figure 8**. Towards the top, the dense encapsulation layer with low Ce and C contents was revealed. The coating is homogeneous through the thickness where Ce, C, Si, and O contents are almost flat as a function of the sputtering time, suggesting no interfacial phase segregation. The C content is ~7% in the film indicating that some organic components are present. These organic components can provide better plasticity and flexibility to the film and can potentially enhance the adhesive properties of the film with polymeric substrates.[4-6] These NC coatings can also be

deposited onto other adhesive layers reported earlier to create bilayer structures with better overall reliability.[6, 33] The atomic percentage of the Ce was determined to be ~2.6% and the calculated nanoparticle weight percentage matches the value (20 wt.%) calculated from the nanoparticle and coating matrix deposition rates.

3. Conclusion

We demonstrate a versatile ultrasonic spray – open air plasma dual source deposition method being capable of making various kinds of multifunctional NC coatings with high nanoparticle loadings. The deposition method eliminates the potential difficulties associated with preparing high mass fraction NC coatings with well-dispersed nanoparticles in the matrix solution and is capable of depositing films with good nanoparticle dispersity and strong nanoparticle-matrix interactions. NC coatings were successfully deposited on various kinds of substrates including polycarbonate at a low processing temperature. Coatings containing SiO_2, CeO_2, and both TiO_2 and CeO_2 nanoparticles were deposited with similar processing conditions and their surface morphologies, optical properties and mechanical properties were systematically reported. The resulting films showed good nanoparticle dispersity, high transparency in the visible wavelength, effective absorption in the UV wavelength, and enhanced mechanical properties compared to the referencing coating matrix. The photostability of the UV-absorbing NC coatings were also determined using an accelerated UV test where the results demonstrated significantly better performance than the existing UV-absorbing composites with either polymeric matrix or organic UV-absorbing molecules. The method demonstrates a new approach for making high performance NC coatings and is adaptable for numerous applications.

4. Experimental Section

Preparation of the Nanoparticle dispersions. Amine-functionalized SiO_2 nanoparticle dispersions in water (25.2 wt.%), CeO_2 nanoparticle dispersions in water (10 wt.%) and TiO_2 nanoparticle dispersions in water (33-37 wt.%) were purchased from Sigma Aldrich. Their size distribution profiles were measured by a DLS instrument (Nanobrook Omni, Brookhaven Instrument Inc., US) after diluted with deionized-water to a concentration of 0.1 wt.% and sonicated for 15 min. Further diluted nanoparticle dispersions were employed for spraying.

Deposition of the NC coatings. The NC coatings were co-deposited with OAPD of the coating matrix and ultrasonic spraying of the functional nanoparticles (**Figure 1**). An OAPD instrument equipped with an atmospheric 13.56 MHz radiofrequency plasma source and a cylindrical plasma showerhead (Atomflow 400D system, Surfx Technologies LLC, US) was used for depositing the coating matrix. Plasma gases consisted of a primary gas of 20 L/min of high purity compressed helium (99.995%, Praxair, US) and a secondary gas of 0.3 L/min of high purity compressed oxygen (99.999%, Praxair, US). The silane precursor, bis(trimethooxysilyl)hexane (99%, Gelest Inc., US), was heated to 130 ℃ and delivered to the after-glow plasma region through a bubbler by a high-temperature precursor delivery system that was previously reported.[6] The precursor molecules then interacted with the plasma afterglow species before being deposited onto the substrate underneath the showerhead.

An ultrasonic spraying system (Sonotek, US) was employed to co-deposit the functional nanoparticles. During spraying, a syringe pump was programmed to a constant infusion rate of 0.3 ml/min and was employed to deliver the nanoparticle dispersions to an ultrasonic nozzle where the liquid gets atomized into a fine mist by 120 kHz, high frequency vibrations. The vibration created by ultrasonic nozzle for atomization also helped the deagglomeration of the

nanoparticles during spraying.[44] The generator power was set to be 1.8 W. A ~ 3 psi nitrogen gas flow was used to direct droplets towards the substrate.

The substrate was placed on a computer controlled motorized translational stage where the translation speed, temperature, and distance can be accurately reproduced. The substrate moved back and forth between two deposition heads for depositing the NC coatings pass-by-pass. The substrate was heated to 80 ℃ during deposition to ensure a complete solvent evaporation before arrival of the plasma. The nanoparticle weight percentage in the final NC coatings were controlled by their weight concentrations in the dispersion during the ultrasonic spraying process including parameters such as the scan speed, solution flow rate, etc. The weight percentage deposited could be estimated from the nanoparticle deposition rate compared to the overall NC coating deposition rate. These estimations were checked by performing SEM following the nanoparticle deposition to determine the nanoparticle content per cycle and by performing profilometry followed by the NC deposition to determine the NC coating thickness. The measured deposited volumes were then converted to weights using their corresponding densities. These estimations were also confirmed with XPS analysis (except for the SiO_2 NC coatings due to the presence of silicon in the coating matrix) and were all within 15% relative difference.

Nanoparticle dispersion of 0.011 mg/ml, 0.025 mg/ml, and 0.043 mg/ml in water were employed for making ~10 wt.%, ~20 wt.% and ~30 wt.% NC coatings on silicon substrate, respectively. For the other substrates, the dispersion concentrations were slightly adjusted to account for the deposition rate of the coating matrix in order to achieve the targeted nanoparticle inclusion concentration. After NC deposition, an encapsulation layer of ~30 nm thick was deposited on top of it to further embed the nanoparticles near the top surface.

Characterization of the NC coatings. A high-resolution SEM (FEI Magellan 400, Thermo Fisher Scientific Inc., US) was employed to characterize the nanostructures and coating surface morphology. An AFM (XE-70, Park Systems, Korea) operated in the tapping mode was used to characterize the surface roughness and topography. Specular transmission spectra were obtained using a UV-vis-NIR spectrophotometer (Cary 6000i, Agilent Technologies Inc., US). A surface profilometer (Veeco Dektak 150, Veeco Instruments Inc., US) was used to measure the film thickness with a film edge created by masking a small region.

The through-thickness chemical composition of the NC coatings were characterized by an XPS (PHI 5000 Versaprobe, Physical Electronics Inc., US) using Al−K_α (1486 eV) X-ray source. The XPS depth profiling was performed using Argon ion beam as the sputtering source. An SAM (PHI 700, Physical Electronics Inc., US) was employed to measure the spatial elemental mapping of the NC coatings. Before the measurements, an Argon pre-sputtering (~100 nm) was employed. Primary electron beam of 25 kV was used as the source for exciting Auger electrons and a mapping area of 5 um * 4 um was scanned with a spatial resolution of 128 points per line.

The films elastic modulus and hardness were measured by a nano-indenter (iNano, Nanomechanics, US) with a diamond tip. A calibration using a standard sample was performed before testing and at least 16 individual points were tested for each specimen. For the accelerated photostability test, NC specimens were irradiated using a mercury based UV-lamp. The measured light power reaching the specimen was ~60 W/m^2 in the UV-B range which is more than 75 times the average UV-B component of sunlight exposure received on Earth (calculated by Modtran 3.7 program).

Acknowledgements

This work was supported by US Department of Energy, Office of Basic Energy Sciences, under Contract No. DE-FG02-07ER46391. Part of this work was performed at the Stanford Nano Shared Facilities (SNSF), supported by the National Science Foundation under award ECCS-1542152.

References

[1] A. Kakaroglou, B. Nisol, K. Baert, I. De. Graeve, F. Reniers, G. Van Asschec, H. Terryna, *RSC Adv.*, 2015, **5**, 27449-27457.

[2] A. Ladwig, S. Babayan, M. Smith, M. Hester, W. Highland, R. Koch, R. Hicks, *Surf. Coat. Technol.*, 2007, **201**, 6460-6464.

[3] L. Bárdos, H. Baránková, *Thin Solid Films*, 2010, **518**, 6705-6713.

[4] S. Dong, J. Han, Z. Zhao, R. H. Dauskardt, *Plasma Process Polym*., 2016, **13**, 1053-1060.

[5] L. Cui, K. Lionti, A. Ranade, K. Larson-Smith, G. Dubois, R. H. Dauskardt, *ACS Nano*, 2014, **8**, 7186-7191.

[6] S. Dong, Z. Zhao, R. H. Dauskardt, *ACS Appl. Mater. Interfaces*, 2015, **7**, 17929-17934.

[7] D. Merche, N. Vandencasteele, F. Reniers, *Thin Solid Films*, 2012, **520**, 4219-4236.

[8] G. Borcia, C. A. Anderson, N. M. D. Brown, *Plasma Sources Sci. Technol.*, 2005, **14**, 259-267.

[9] L. Cui, A. N. Ranade, M. A. Matos, G. Dubois, R. H. Dauskardt, *ACS Appl. Mater. Interfaces*, 2013, **5**, 8495-8504.

[10] L. Sowntharya, R. C. Gundakaram, K. R. C. S. Raju, R. Subasri, *Ceram. Int.*, 2013, **39**, 4245-4252.

[11] H. Schmidt, *Appl. Organomet. Chem.*, 2001, **15**, 331-343.

[12] A. Chen, P. H. Hindle, *Chem. Rev.*, 2010, **110**, 3767-3804.

[13] J. A. Trindell, J. Clausmeyer, R. M. Crooks, *J. Am. Chem. Soc.*, 2017, **139**, 16161-16167.

[14] F. Caputo, M. D. Nicola, A. Sienkiewicz, A. Giovanetti, I. Bejarano, S. Licoccia, E. Traversa, L. Ghibelli, *Nanoscale*, 2015, **7**, 15643-15656.

[15] N. N. Dao, M. D. Luu, Q. K. Nguyen, B. S. Kim, *Adv. Nat. Sci.: Nanosci. Nanotechnol.*, 2011, **2**, 045013-045016.

[16] M. Ferrari, *Nat. Rev. Cancer*, 2005, **5**, 161-171.

[17] L. Chen, S. Xiao, H. Zhu, L. Wang, H. Liang, *Soft Matter*, 2016, **12**, 2632-2641.

[18] L. Luo, Z. Duan, H. Li, J. Kim, G. Henkelman, R. M. Crooks, *J. Am. Chem. Soc.*, 2017, **139** 5538-5546.

[19] L. Bai, X. Wang, Q. Chen, Y. Ye, H. Zheng, J. Guo, Y. Yin, C. Gao, *Angew. Chem. Int. Ed.*, 2016, **55**, 15656-15661.

[20] D. Guo, G. Xie, J. Luo, *J. Phys. D: Appl. Phys.*, 2014, **47**, 013001.

[21] L. Bu, N. Zhang, S. Guo, X. Zhang, J. Li, J. Yao, T. Wu, G. Lu, J. Ma, D. Su, *Science*, 2016, **354**, 1410-1414.

[22] G. Siqueira, J. Bras, A. Dufresne, *Biomacromolecules*, 2009, **10**, 425-432.

[23] W. Francisco, F. V. Ferreira, E. V. Ferreira, L. Cividanes, A. Coutinho, G. Thim, *J. Aerosp. Technol. Manag.*, 2015, **7**, 289-293.

[24] B. Ramezanzadeh, M. Mohseni, A. Karbasi, *J. Mater. Sci.*, 2012, **47**, 440-454.

[25] T. Hübert, H. Hattermann, M. Griepentrog, *J. Sol-Gel Sci. Technol.*, 2009, **51**, 295-300.

[26] M. I. Barrena, J. M. Gómez de Salazar, A. Soria, R. Canas, *Appl. Surf. Sci.*, 2014, **289**, 124-128.

[27] V. Baldim, F. Bedioui, N. Mignet, I. Margaill, J. F. Berret, *Nanoscale*, 2018, **10**, 6971-6980.

[28] S. Cho, C. Ahn, J. Park, S. Jeon, *Nanoscale*, 2018, **10**, 9747-9751.

[29] W. Ouyang, F. Teng, X. Fang, *Adv. Funct. Mater.*, 2018, **28**, 1707178.

[30] P. K. Mishra, R. Kumar, P. K. Rai, *Nanoscale,* 2018, **10**, 7257-7269.

[31] G. S. Lonakar, M. S. Mahajan, S. S. Ghosh, J. V. Sali, *Org. Electron.*, 2012, **13**, 2575-2581.

[32] C. Katsoulis, E. Kandare, B. K. Kandola, *Polym. Degrad. Stab.*, 2011, **96**, 529-540.

[33] Y. Ding, S. Dong, J. Han, D. He, Z. Zhao, R. H. Dauskardt, *Adv. Mater. Inter.*, 2018, **5**, 1701433.

[34] K. Terpilowski, D. Rymuszka, O. V. Goncharuk, I. Ya. Sulym, V. M. Gun'ko, *Appl. Surf. Sci.*, 2015, **353**, 843-850.

[35] A. Batan, N. Mine, B. Douhard, F. Brusciotti, I. De Graeve, J. Vereecken, M. Wenkin, M. Piens, H. Terryn, J. J. Pireaux, F. Reniers, *Chem. Phys. Lett.*, 2010, **493**, 107-112.

[36] R. K. Goyal, A. S. Kapadia, *Compos. Part B-Eng.*, 2013, **50**, 135-143.

[37] Z. Chen, L. Y. L. Wu, E. Chwa, O. Tham, *Mater. Sci. Eng. A Struct. Mater.*, 2008, *493*, 292.

[38] N. Bail, S. Benayoun, B. Toury, *J. Sol-Gel Sci. Technol.*, 2015, **75**, 710-719.

[39] D. A. Banerjee, A. J. Kessman, D. R. Cairns, K. A. Sierros, *Surf. Coat. Technol.*, 2014, **260**, 214-219.

[40] P. G. Parejo, M. Zayat, D. Levy, *J. Sol-Gel Sci. Technol.*, 2010, **53**, 280-286.

[41] T. Soitong, S. Wongsaenmai, *Key Eng. Mater.*, 2017, **751**, 796-800.

[42] A. L. Linsebigler, G. Lu, J. T. Yates, *Chem. Rev.*, 1995, **95**, 735-758.

[43] J. Bardon, J. Bour, D. D. Frari, C. Arnoult, D. Ruch, *Plasma Process Polym*., 2009, **6**, S655-S659.

[44] R. M. Rodgers, H. Mahfuz, V. K. Rangari, N. Chisholm, S. Jeelani, *Macromol. Mater. Eng.*, 2005, **290**, 423-429.

Table 1 Processing conditions for NC coating deposition

Parameter	Unit	Value
OAPD		
Primary plasma gas		He (99.995%)
Secondary plasma gas		O_2 (99.995%)
Bubbler and dilution gas		He (99.995%)
Precursor temperature	°C	130
Primary gas flow	L min^{-1}	20
Secondary gas flow	L min^{-1}	0.3
Bubbler gas flow	L min^{-1}	0.15
Dilution gas flow	L min^{-1}	2.0
Plasma power	W	70
Deposition distance	mm	3
Ultrasonic Spraying		
Generator power	W	1.8
Solution flow rate	mL min^{-1}	0.3
Deposition distance	cm	8
Nitrogen pressure	psi	3
Translational Stage		
Temperature	°C	80
Scan speed (X-direction)	cm s^{-1}	5
Scan range (X-direction)	mm	240
Step size (Y-direction)	mm	0.3

Figures

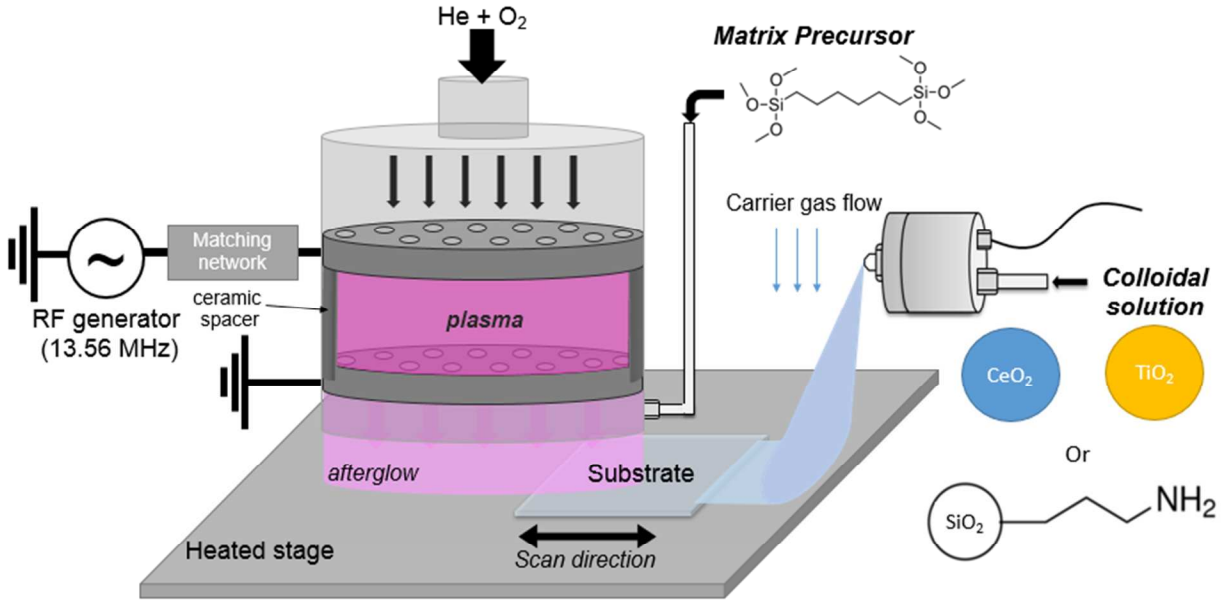

Figure 1. Molecular structures of the employed chemical precursors and a schematic illustrating the instrument setup for the dual-source spray-OAPD method

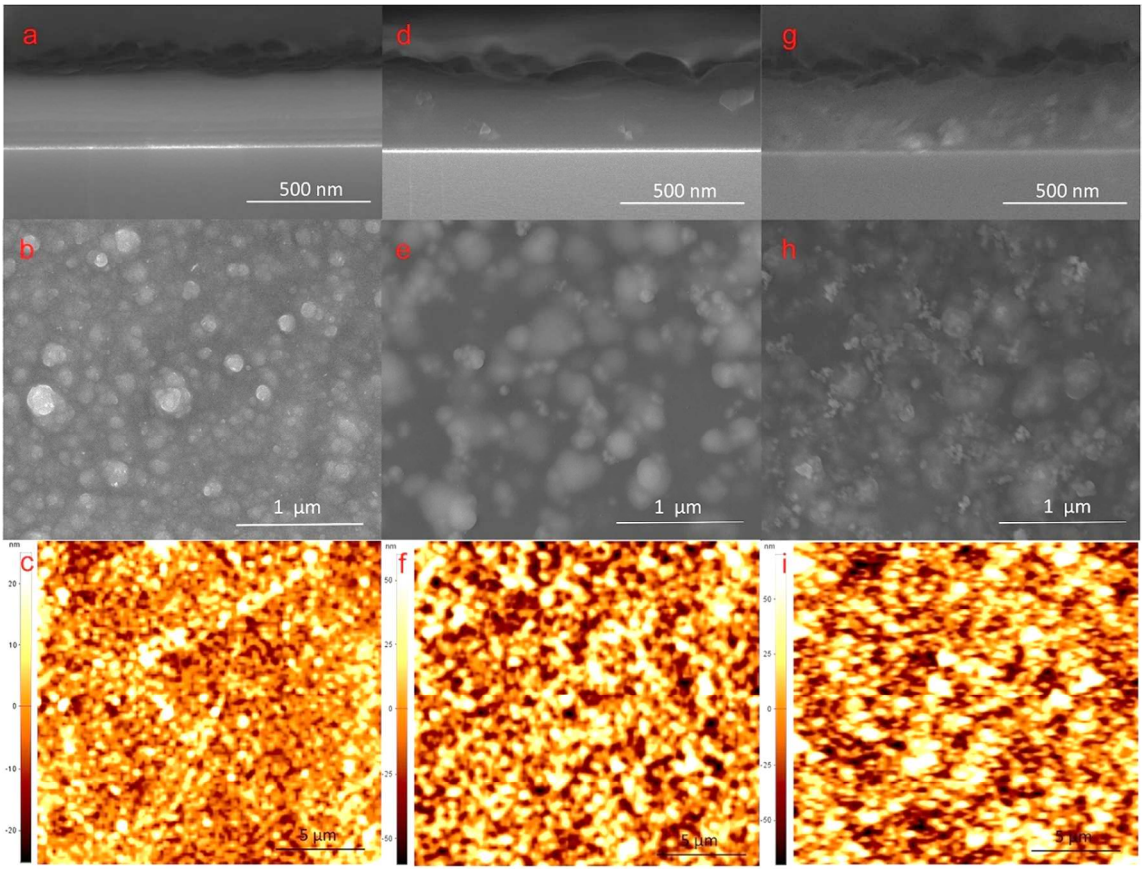

Figure 2. Surface morphology of the NC coatings containing (a - c) 20 wt.% SiO_2, (d - e) 20 wt.% CeO_2, and (g – i) 10 wt.% TiO_2 + 10 wt.% CeO_2 nanoparticles deposited on silicon substrates

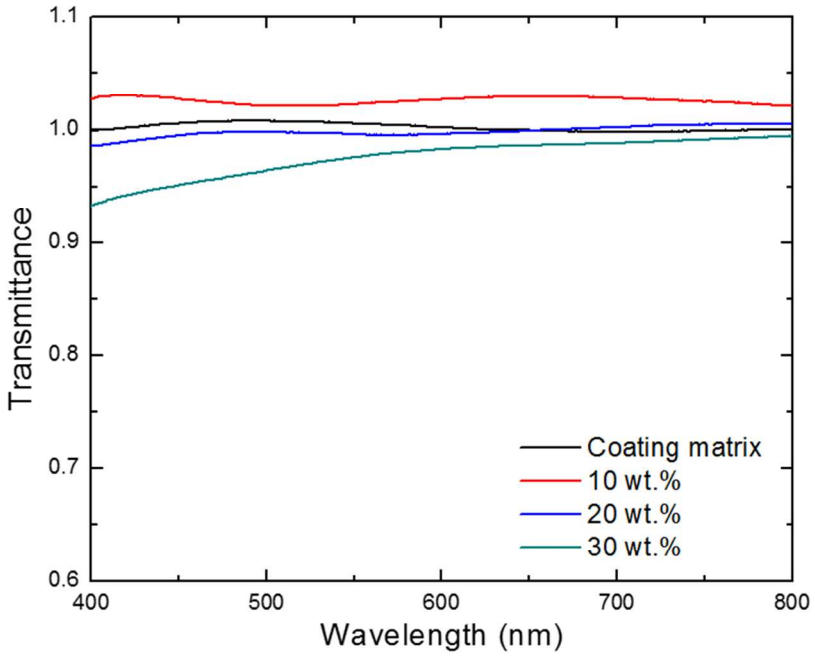

Figure 3. Transmittance of the SiO_2 NC coatings on glass containing different concentrations of nanoparticles

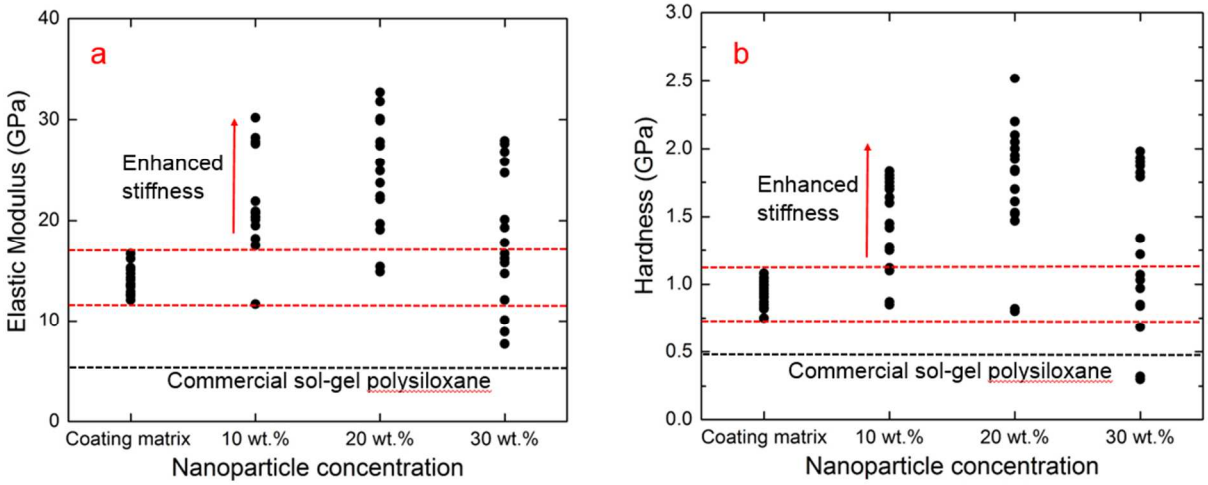

Figure 4. (a) Elastic modulus and (b) hardness of the SiO_2 NC coatings containing different concentrations of nanoparticles

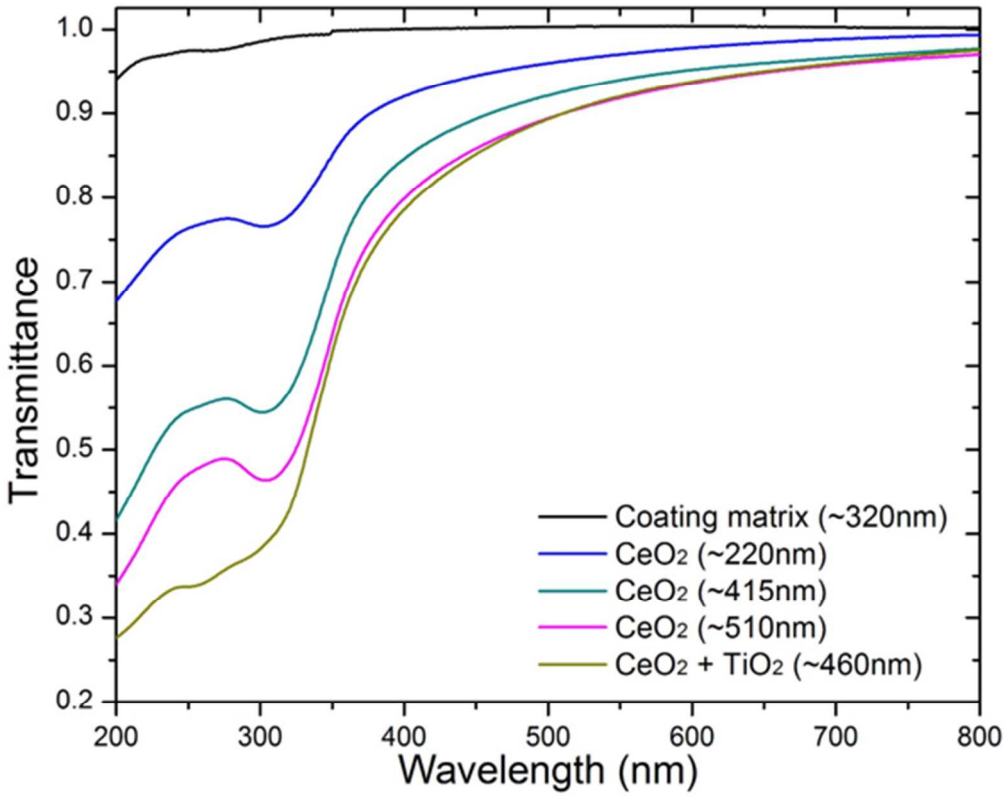

Figure 5. Transmittance of the coating matrix (no nanoparticle inclusion) and UV-absorbing NC coatings containing either 20 wt.% CeO_2 or 10 wt.% CeO_2 + 10 wt.% TiO_2 nanoparticles with varying film thicknesses

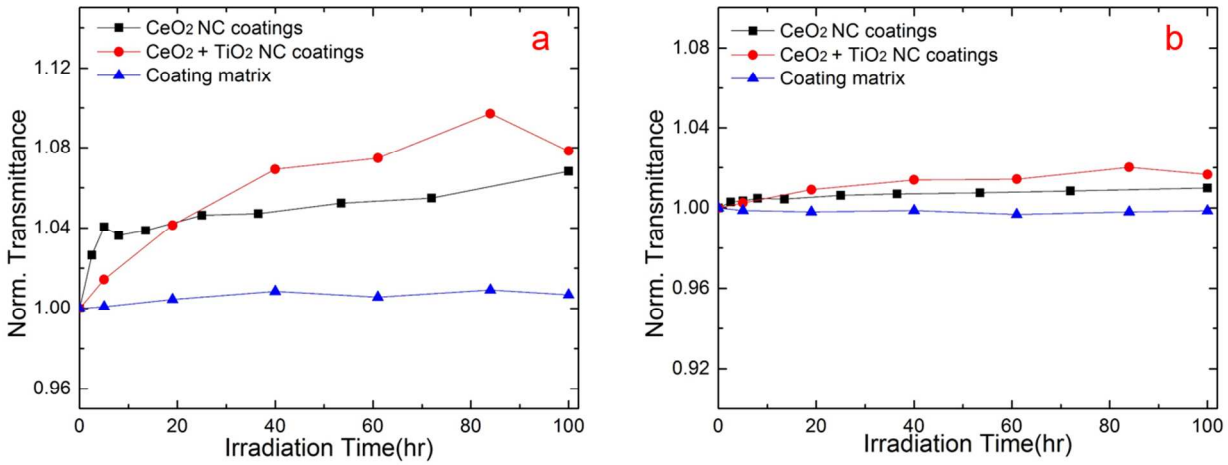

Figure 6. Photostability of the UV-absorbing NC coatings containing either 20 wt.% CeO_2 or 10 wt.% CeO_2 + 10 wt.% TiO_2 nanoparticles under accelerated UV test. Normalized transmittance at wavelength of (a) 305 nm and (b) 550 nm is plotted as a function of the irradiation time.

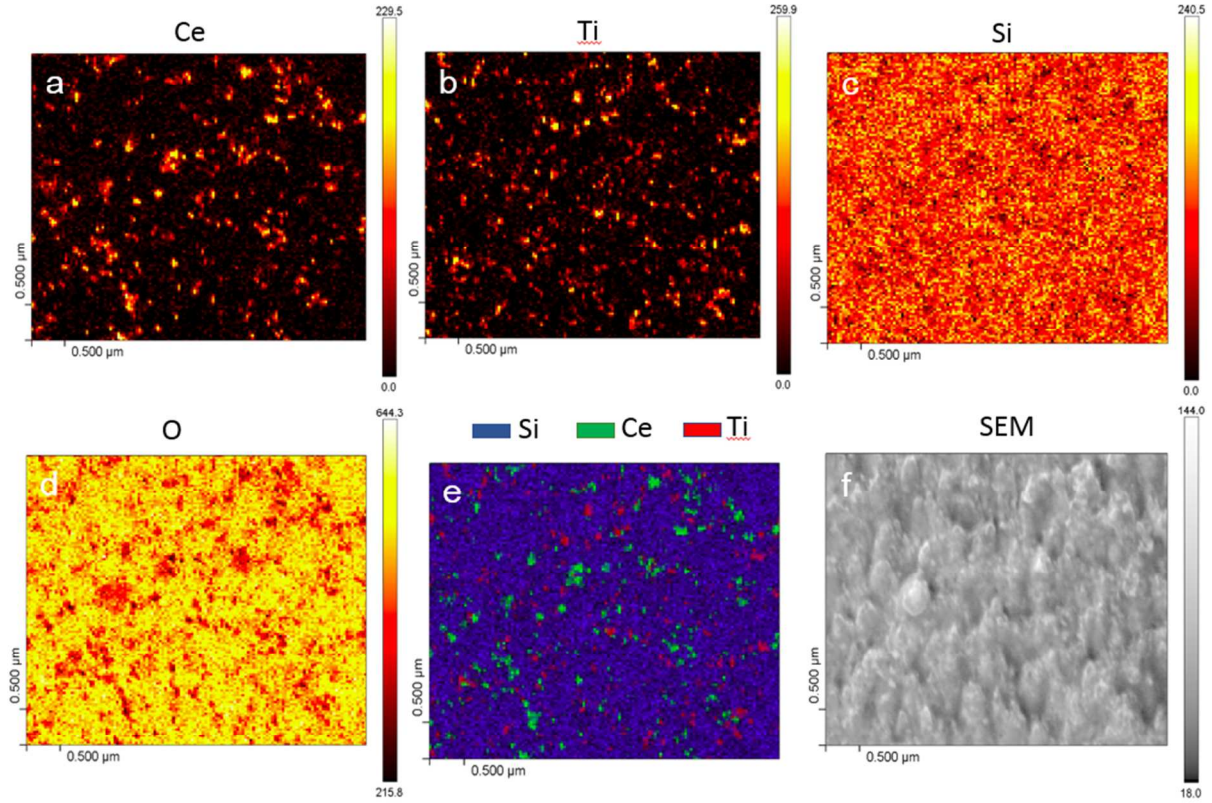

Figure 7. (a - e) SAM elemental mapping of NC coatings on silicon substrate containing 10 wt.% TiO_2 + 10 wt.% CeO_2 nanoparticles together with the (f) corresponding SEM image of the scanned area

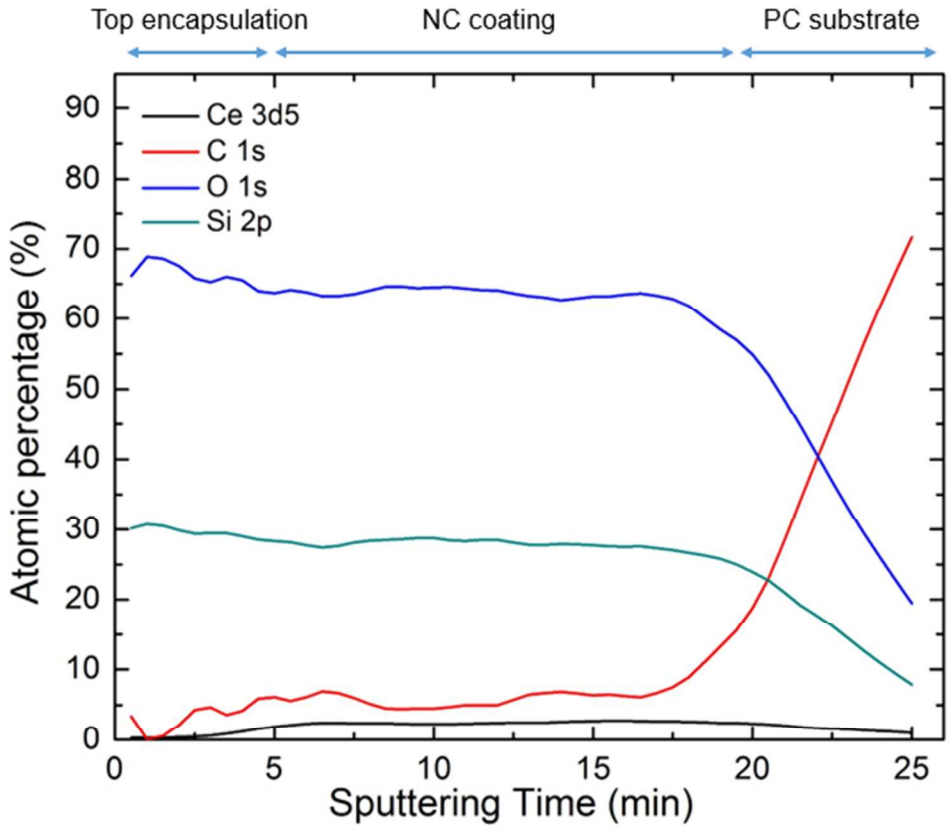

Figure 8. XPS depth profile of NC coatings containing 20 wt.% of CeO_2 nanoparticles deposited on a PC substrate

Table of content

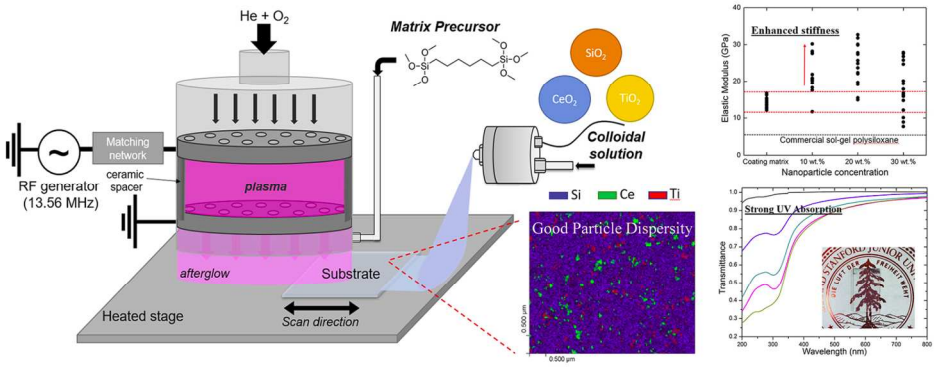

Mechanically robust UV-absorbing nanocomposite coatings with good nanoparticle uniformity and dispersity were deposited using a versatile dual-source deposition method